Pressure-induced cation-cation bonding in V_2O_3

Ligang Bai,[1,2,*] Quan Li,[2] Serena A. Corr,[3] Michael Pravica,[2] Changfeng Chen,[2] Yusheng Zhao,[2] Stanislav V. Sinogeikin,[1] Yue Meng,[1] Changyong Park,[1] and Guoyin Shen[1,†]

[1]*High Pressure Collaborative Access Team (HPCAT), Geophysical Laboratory, Carnegie Institute of Washington, Argonne, Illinois 60439, USA*

[2]*Department of Physics and Astronomy, University of Nevada Las Vegas and High Pressure Science and Engineering Center (HiPSEC), Las Vegas, Nevada 89154-4002 USA*

[3]*School of Chemistry, University of Glasgow, Glasgow G12 8QQ, United Kingdom*

(Received 9 January 2014; revised manuscript received 17 June 2015; published 9 October 2015)

A pressure-induced phase transition, associated with the formation of cation-cation bonding, occurs in V_2O_3 by combining synchrotron x-ray diffraction in a diamond anvil cell and *ab initio* evolutionary calculations. The high-pressure phase has a monoclinic structure with a $C2/c$ space group, and it is both energetically and dynamically stable at pressures above 47 GPa to at least 105 GPa. This phase transition can be viewed as a two-dimensional Peierls-like distortion, where the cation-cation dimer chains are connected along the c axis of the monoclinic cell. This finding provides insights into the interplay of electron correlation and lattice distortion in V_2O_3, and it may also help to understand novel properties of other early transition-metal oxides.

DOI: 10.1103/PhysRevB.92.134106 PACS number(s): 64.70.K−, 61.50.Ks, 62.50.−p, 63.20.D−

Properties of early transition-metal (Ti,V,Cr) oxides are strongly influenced by two well-known competing mechanisms. One is the strong electron-electron correlation (Mott-Hubbard) mediated by a weak cation-cation interaction, with the other being the cation-cation bonding (Peierls distortion) through strong cation interactions when these cations are located in edge- or face-sharing octahedra [1–4]. The cooperation and competition of these two effects are sensitive to conditions such as doping, temperature, and pressure [5–15]. Understanding the roles of each condition parameter and the mechanisms governing the rich and interesting properties is of fundamental significance. Pressure as an external parameter can suppress the strong electron-electron correlation effect by broadening the bandwidth [16,17], and it may activate or enhance dimerization by reducing atomic distances [18,19]. Indeed, the dimerization between two cations has been observed in TiOCl and MnS_2 under high pressures [3,4,20].

Vanadium sesquioxide (V_2O_3) is the only transition-metal sesquioxide that displays metallic nature at ambient condition among others (e.g., Cr_2O_3, Fe_2O_3, Ti_2O_3, etc.), and it is often referred to as a typical Mott-Hubbard material, where electron-electron correlation plays an important role [5,21,22]. It crystallizes in the hexagonal corundum-type structure, with V ions (V^{3+}, $3d^2$) occupying face-sharing octahedra along the c axis and edge-sharing octahedra in the basal plane. At ambient condition, V_2O_3 is a paramagnetic metal. Upon cooling down to 150 K, V_2O_3 undergoes a first-order metal-insulator transition (MIT) accompanied by a monoclinic structural distortion and a transition to antiferromagnetic phase due to strong electron-electron correlation [23–27]. On the other hand, the dimerization was proposed in V_2O_3 based on the Heisenberg model decades ago [28], where pairwise bonding and antiferromagnetism were viewed as two possibilities on the basal honeycomb plane of V_2O_3. Recently, dimerization between V ions has been observed in the basal plane of single-crystal (0001) thin films [29].

By applying pressure, the MIT in V_2O_3 was found to be gradually diminished and eventually disappear at 2.6 GPa [5]. Recently, a new high-pressure phase of V_2O_3 was reported by several groups. Ovsyannikov *et al.* [30] proposed an orthorhombic Rh_2O_3(II) structure for the high-pressure phase. Zhang *et al.* [31] reported a monoclinic distortion above 31 GPa. Ding *et al.* [32] suggested that this high-pressure monoclinic phase is similar to the low-temperature monoclinic phase. In this paper, we report results from synchrotron x-ray powder diffraction experiments and *ab initio* swarm intelligence calculations. These results lead to the determination of a high-pressure phase of V_2O_3 that contains zigzag chains of vanadium dimers, which is different from the structure at low temperature. This structural characterization provides insights into the interplay of electron correlation and lattice distortion in V_2O_3, and it may also help to understand novel properties of other early transition-metal oxides in general.

A high-purity V_2O_3 sample (see synthesis details in [33]) was loaded into a 100 μm hole of a 35-μm-thick preindented rhenium gasket. Pressure was generated by a symmetric diamond anvil cell (DAC) with a diamond culet diameter of 300 μm. The pressure was determined by the ruby fluorescence method [34]. Helium and neon were used as pressure-transmitting media, and samples were loaded at room temperature by using a high-pressure gas-loading system [35]. Angle-dispersive x-ray diffraction (XRD) data were collected at beamlines 16-ID-B and 16-BM-D of the High Pressure Collaborative Access Team (HPCAT) at the Advance Photon Source, Argonne National Laboratory. The x-ray beam size was about $5(v) \times 7(h)$ μm^2 at full width at half-maximum (FWHM), with a wavelength of 0.4066 Å [36]. Diffraction patterns were recorded using MAR-CCD or Pilatus detectors with exposure times between 10 and 60 s. The structural refinements were performed using the Rietveld refinement program FULLPROF [37] and GSAS [38].

In the first experimental run up to 18.9 GPa, helium was used as the pressure-transmitting medium providing a

*lbai@ciw.edu
†gshen@ciw.edu

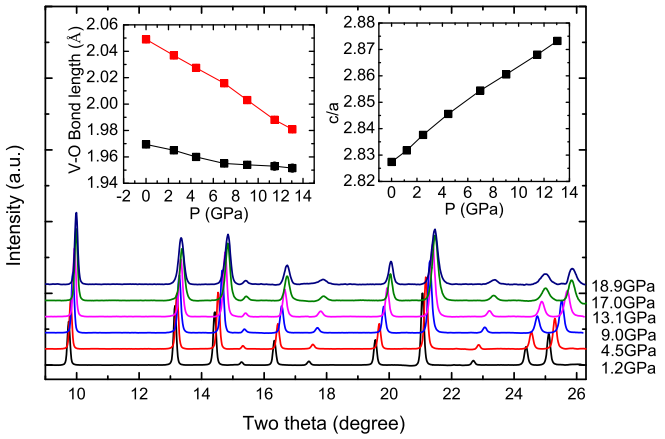

FIG. 1. (Color online) Pressure evolution of diffraction profile in a helium medium. Left inset: compression of the V-O bonds up to 13 GPa. The standard deviations of bond lengths and c/a are less than the size of the symbols. Right inset: pressure evolution of the axial ratio.

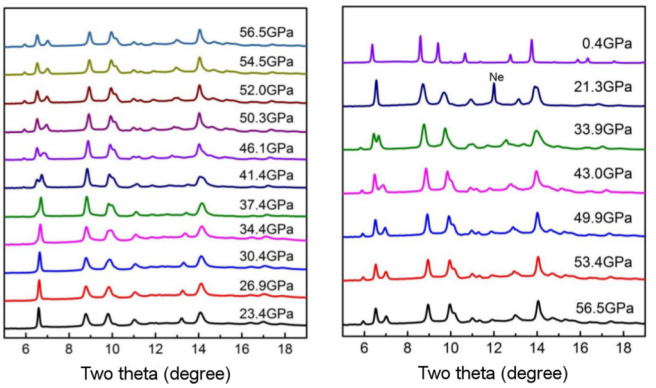

FIG. 2. (Color online) X-ray diffraction patterns of V_2O_3 as a function of pressure at room temperature (left panel, compression; right panel, decompression).

hydrostatic condition up to 20 GPa [39] and a quasihydrostatic condition at higher pressures. No phase transition is observed up to 18.9 GPa, as shown in Fig. 1. Below 13.1 GPa, the quality of diffraction patterns is well suited for Rietveld refinements, yielding the lattice parameters and atomic positions. At pressures above 13.1 GPa, determining atomic positions becomes difficult, and only lattice parameters are extracted from the diffraction patterns. Fitting the pressure dependence of the volume below 18.9 GPa to the Birch-Murnaghan equation gives a bulk modulus $B = 197(1)$ GPa, in general agreement with previous reports [40–42]. The compression is anisotropic with the c/a ratio increasing with increasing pressure, which is unique for V_2O_3 among the isostructural sesquioxides, but it is consistent with the results of previous studies [32,41–43].

In this phase of V_2O_3 at low pressures, the V ions in the corundum structure are located in VO_6 octahedra with a small trigonal distortion that causes the splitting of the t_{2g} shell into an a_{1g} orbital oriented along the c axis and two degenerated e_g orbitals on the ab plane. This trigonal distortion splits the six V-O distances into two distinct groups. As shown in Fig. 1, the difference between these two groups decreases sharply with increasing pressure, which means that the V^{3+} ion moves closer to the center of the VO_6 octahedra, thereby reducing trigonal distortion with increasing pressure. The reduction of the trigonal distortion will reduce the splitting of the e_g and a_{1g} orbitals and hence increase the hybridization between them, thus weakening the electron correlation energy (U). Furthermore, the bandwidth (W) will be broadened with increasing pressure associated with reduced interatomic distances. Therefore, the effective correlation effect (U/W) will be largely reduced by pressure, consistent with the progressively diminishing MIT observed under pressure [5].

In the second run, we used neon as a pressure-transmitting medium for experiments at higher pressures, and we observed a new high-pressure phase, as shown in Fig. 2. A typical x-ray diffraction image of the high-pressure phase is shown in Fig. S1. The phase transition is rather sluggish, spanning a pressure range from 30.4 to 50.3 GPa. Upon pressure release from 56.5 GPa, a hysteresis of 10 GPa is observed. As shown in Fig. 2, the diffraction lines of the new phase are relatively broad due to possible uniaxial stress in the pressure range even with neon medium [39]. We attempted to use the laser-heating technique to anneal the samples. However, for laser-heated samples at temperatures below 1200 K, no clear change was found in the diffraction peak width. At temperatures above 1200 K, the V_2O_3 sample transformed into a new high-temperature phase.

The diffraction pattern at 50.3 GPa can be indexed into a monoclinic cell. The overall quality of the diffraction pattern is not sufficient to solve the atomic positions. To refine the structure of this new phase, we used a monoclinic cell (space group $I2/a$, No. 15) similar to the low-temperature phase of V_2O_3 as an initial model for Rietveld refinements. The refinement procedures were performed by using FULLPROF and GSAS. It is found that Rietveld results display uncertainties, with the atomic positions of vanadium and oxygen varying with the choices of software packages or the refinement procedures (see Note-1 in the supplemental material [44]), possibly due to the preferred orientation caused by textures under uniaxial stress and peak broadening effect caused by the microscopic deviatoric stress field. Because Rietveld refinement alone cannot unambiguously determine the structure of the new phase, we performed variable-cell structure prediction simulations using the CALYPSO [45–48] methodology containing one, two, and four formula units (f.u.) in the pressure range of 40–100 GPa. Analysis of the predicted and experimental x-ray diffraction patterns (see Fig. S2 in [44]) reveals an intriguing monoclinic structure with 2 f.u. (10 at/cell) per unit cell and a space group of $C2/c$ (another setting of space group 15) with the V ions located on the $8f$ (x,y,z) sites, and the O anions on the $8f$ (x,y,z) and $4e$ $(0,y,0.75)$ sites. The results in Fig. 3(a) show that the simulated XRD pattern, considering the preferred orientation effect, of the predicted high-pressure V_2O_3 is in good agreement with the experimental XRD pattern (see Note-2 in the supplemental material [44]). The small difference in intensity could be due to the preferred orientation arising from uniaxial stress. Although our theoretical simulations and Rietveld refinements give slightly different atomic positions (see Table S2 in [44]), we note that both results lead to a framework of a monoclinic structure [Fig. 3(b) and Table S3 in [44]] that contains two

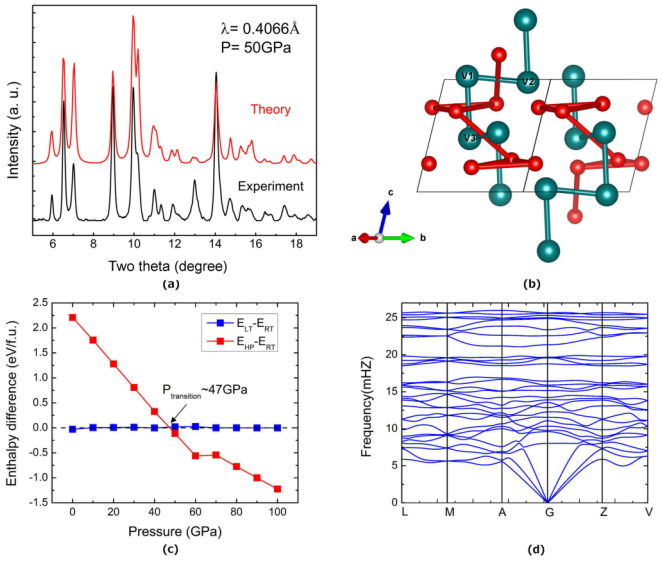

FIG. 3. (Color online) (a) Comparison of theoretical and experimental x-ray powder diffraction patterns of the high-pressure phase V_2O_3. (b) The V-V bond structure in high-pressure monoclinic V_2O_3. The teal and red balls represent the vanadium and oxygen atoms, respectively. (c) The pressure evolution in the relative enthalpies of high-pressure and low-temperature monoclinic structures from static calculations. The dashed line indicates zero enthalpy difference. (d) Phonon-dispersion curves for the high-pressure monoclinic structure at 50 GPa.

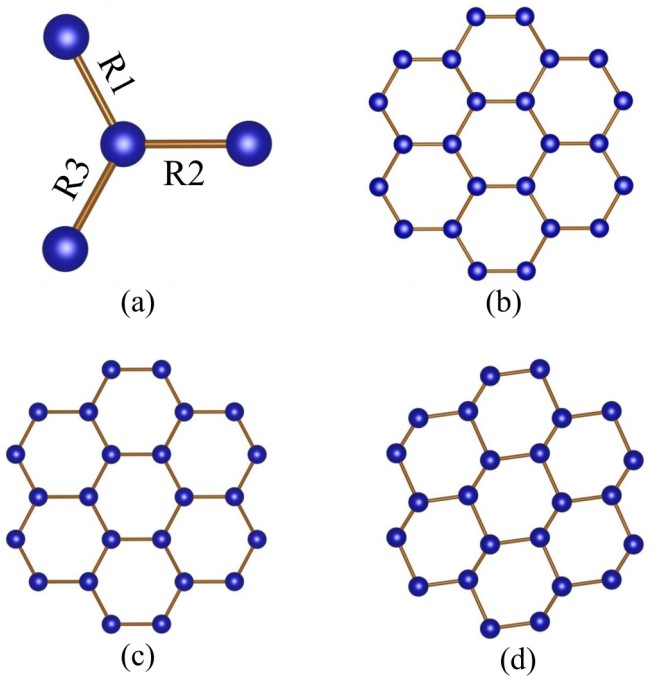

FIG. 4. (Color online) (a) Each vanadium atom in V_2O_3 has three nearest neighbors with three bond lengths ($R1$, $R2$, and $R3$), with blue spheres representing the vanadium atom. The puckered honeycomb lattices in the basal plane for (b) the room-temperature phase with $R1 = R2 = R3$, (c) the low-temperature phase with $R2 > R1 \approx R3$ below 150 K, and (d) the high-pressure phase with $R3 < R2 < R1$ above 47 GPa. For simplicity, oxygen atoms are not shown.

shortest V-V distances, namely the V1-V2 pairs in the basal plane with edge-sharing octahedra and the V1-V3 pairs along the c axis with face-sharing octahedra. In this way, vanadium pairs are connected in a zigzag pattern forming V-V dimer chains running along the c axis of the monoclinic cell.

To account for the energetic and dynamic stability of this new monoclinic structure, we performed calculations with the PBE-GGA potential as implemented in the VASP code [49]. The electron-ion interaction was described by means of a projector augmented wave with $3p^6 3d^4 4s^1$ and $2s^2 2p^4$ electrons as valence for V and O atoms, respectively. We used an energy cutoff of 1000 eV for all cases, a Monkhorst-Pack k-point mesh with a grid of $6 \times 6 \times 6$ for Brillouin zone sampling for the structural optimization, and a denser $13 \times 13 \times 13$ mesh for the electronic calculations. The lattice parameters and atomic positions of the low-temperature (LT), room-temperature (RT), and high-pressure (HP) phases were optimized to minimize the forces in the pressure range of 0–100 GPa. Figure 3(c) shows the relative enthalpies of these phases, and in the entire pressure range the trigonal RT and monoclinic LT structure are very close in enthalpy because they differ by only a small distortion. The new HP phase is energetically favorable at pressures higher than 47 GPa, which is in agreement with our experimental results. We also calculated phonon-dispersion curves at 50 GPa using the supercell ($2 \times 2 \times 2$) method. Figure 3(d) shows no imaginary frequency in the entire Brillouin zone, indicating that the HP phase is dynamically stable.

The HP monoclinic phase is similar to the LT monoclinic phase in that they both display the same space group and Wyckoff positions. In fact, the stacking patterns of VO_6 octahedra, i.e., edge-sharing with three others in the basal plane and face-sharing along the c axis, are identical for the RT, HP, and LT phases. The main structural difference lies in the degree of the distortion, which can be viewed by the bonding formation in the basal plane in a pseudo triangular lattice. As shown in Fig. 4, within the basal plane of the corundum structure, the cations are packed into the two-dimensional lattice of the honeycomb structure. The basal plane has threefold rotation symmetry in the RT phase with the three V-V bonds having the same length. The LT phase displays a modest distortion caused by a Jahn-Teller-like lattice instability through the electron-lattice coupling, with one of three bonds slightly elongated and the other two bonds slightly contracted [Fig. 4(c)]. In contrast, the HP phase has a strong distortion with one of three bonds contracted and the other two elongated [Fig. 4(d)]. As discussed above, the compression effect in V_2O_3 is first reflected by a decrease in the trigonal distortion, reducing the effective correlation effect (U/W) and progressively diminishing the MIT. At higher pressures, the large reduction of the V-V distances via a phase transition eventually leads to the formation of the V-V dimer chains. These dimers are periodically distributed in the basal plane and connected along the c axis of the monoclinic cell. The above discussion can also be understood in the model proposed by Nebenzahl based on the Heisenberg model [28], where a competition mechanism between antiferromagnetism against V-V bonding was proposed for V_2O_3.

We calculated the electronic density of states (DOS) for the HP phase (see Note-3 in the supplemental material [44]), and we defined the orbitals α (-2.8 to -0.7 eV) and β (-0.7 to

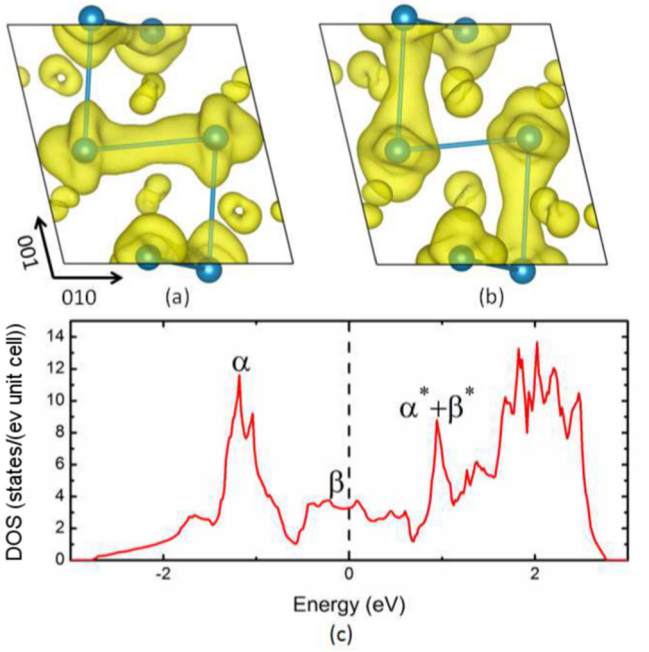

FIG. 5. (Color online) The partial charge densities and density of states (DOS) of the high-pressure phase V_2O_3 at 50 GPa. The isosurfaces of the partial charge densities in the HP phase V_2O_3 are shown for (a) the energy range of -2.8 to -0.7 eV at the isosurface level of 0.03 $e/\text{Å}^3$, and (b) the energy range of -0.7 to 0 eV at the isosurface level of 0.007 $e/\text{Å}^3$. Only the V atom are shown (blue spheres). For simplicity, oxygen atoms are not shown. (c) The total DOS of the HP phase V_2O_3 at 50 GPa. α,β and α*,β* represent bonding and antibonding orbitals, respectively.

0 eV) from the partial charge density distributions, as shown in Figs. 5(a) and 5(b). The two α and β states can be interpreted as bonding in the hexagonal a-b plane (edge-sharing) and along the c axis (face-sharing), respectively. Two sets of bonding-antibonding orbitals (α and α*, β and β*) are clearly visible. The bonding states are separated in the valence band, while the antibonding states are hybridized in the conduction band. The DOS at the Fermi level (D_f) is only contributed by the electrons along the c axis. The partial DOS also shows similar results (see Fig. S5 in [44]), indicating that electrons forming the face-sharing V-V bonding along the c axis are itinerant, while those in the edge-sharing V-V bonding in the a-b plane are pinned below the Fermi level. It should be noted that the D_f in the HP phase is lower than that in the corundum phase (see Fig. S6 in [44]), which could result in a reduction of the electrical conductivity in the HP phase. This is consistent with the recent report by Ding *et al.* [32], where an increase in resistance was observed at high pressures. Recently, Guo *et al.* showed that certain hybrid functionals can describe very well the ambient phases of V_2O_3 [50,51]. For comparison, we also performed band-structure calculations using GGA, GGA+U, and HSE functionals, which produced similar results (see Fig. S7 in [44]).

In summary, we have performed a combined experimental and theoretical study to understand the interplay between electron correlations and Peierls distortions in V_2O_3 under high pressure. While the metal-insulator transition of V_2O_3 at low temperature (150 K) may be largely related to strong electron correlation interactions and orbital ordering, the compression causes band broadening and reducing trigonal distortion that suppresses the correlation effect and orbital ordering. At higher pressures, a phase transition is observed, with the high-pressure phase characterized by the formation of the V-V dimers that can be viewed as a two-dimensional Peierls-like distortion. The high-pressure monoclinic V_2O_3 structure identified here has not been seen in any other transition-metal sesquioxides. This finding provides important insights into the interplay between electron correlations and Peierls distortions, and it may also help to explore other early transition-metal oxides, such as Cr_2O_3.

We thank Yand Ding for helpful discussions. This work used the gas loading setup at GSECARS and the beamline at HPCAT (Sector 16), both located at Advanced Photon Source, Argonne National Laboratory. HPCAT operations are supported by DOE-NNSA under Award No. DE-NA0001974 and DOE-BES under Award No. DE-FG02-99ER45775, with partial instrumentation funding by the NSF. Use of the Advanced Photo Source is supported by the DOE Office of Science, Office of Basic Energy Sciences, under Contract No. DE-AC02-06CH11357. Work at UNLV is supported by DOE-NNSA under Award No. DE-NA001982.

[1] N. F. Mott, *Metal-Insulator Transitions*, 2nd ed. (Taylor & Francis, London, 1990).
[2] J. B. Goodenough, Phys. Rev. **117**, 1442 (1960).
[3] Y.-Z. Zhang, H. O. Jeschke, and R. Valentí, Phys. Rev. Lett. **101**, 136406 (2008).
[4] S. Blanco-Canosa, F. Rivadulla, A. Piñeiro, V. Pardo, D. Baldomir, D. I. Khomskii, M. M. Abd-Elmeguid, M. A. López-Quintela, and J. Rivas, Phys. Rev. Lett. **102**, 056406 (2009).
[5] D. B. McWhan, T. M. Rice, and J. P. Remeika, Phys. Rev. Lett. **23**, 1384 (1969).
[6] R. M. Moon, J. Appl. Phys. **41**, 883 (1970).
[7] A. Menth and J. P. Remeika, Phys. Rev. B **2**, 3756 (1970).
[8] D. B. McWhan, A. Menth, J. P. Remeika, W. F. Brinkman, and T. M. Rice, Phys. Rev. B **7**, 1920 (1973).
[9] M. Marezio, D. B. McWhan, J. P. Remeika, and P. D. Dernier, Phys. Rev. B **5**, 2541 (1972).
[10] A. Jayaraman, D. B. McWhan, J. P. Remeika, and P. D. Dernier, Phys. Rev. B **2**, 3751 (1970).
[11] D. B. McWhan and T. M. Rice, Phys. Rev. Lett. **22**, 887 (1969).
[12] S. A. Corr, D. P. Shoemaker, B. C. Melot, and R. Seshadri, Phys. Rev. Lett. **105**, 056404 (2010).
[13] P. Pfalzer, G. Obermeier, M. Klemm, S. Horn, and M. L. denBoer, Phys. Rev. B **73**, 144106 (2006).
[14] L. Bai, Q. Li, S. A. Corr, Y. Meng, C. Park, S. V. Sinogeikin, C. Ko, J. Wu, and G. Shen, Phys. Rev. B **91**, 104110 (2015).
[15] A. Zylbersztejn, Phys. Rev. B **11**, 4383 (1975).
[16] F. Nakamura, T. Goko, M. Ito, T. Fujita, S. Nakatsuji, H. Fukazawa, Y. Maeno, P. Alireza, D. Forsythe, and S. R. Julian, Phys. Rev. B **65**, 220402 (2002).

[17] J. R. Patterson, C. M. Aracne, D. D. Jackson, V. Malba, S. T. Weir, P. A. Baker, and Y. K. Vohra, Phys. Rev. B **69**, 220101 (2004).
[18] Z. Sun, J. Zhou, H.-K. Mao, and R. Ahuja, Proc. Natl. Acad. Sci. (USA) **109**, 5948 (2012).
[19] Y. Yao and D. D. Klug, Phys. Rev. B **81**, 140104 (2010).
[20] S. A. J. Kimber, A. Salamat, S. R. Evans, H. O. Jeschke, K. Muthukumar, M. Tomić, F. Salvat-Pujol, R. Valentí, M. V. Kaisheva, I. Zizak, and T. Chatterji, Proc. Natl. Acad. Sci. (USA) **111**, 5106 (2014).
[21] N. F. Mott, Rev. Mod. Phys. **40**, 677 (1968).
[22] C. Castellani, C. R. Natoli, and J. Ranninger, Phys. Rev. B **18**, 5001 (1978).
[23] F. Mila, R. Shiina, F.-C. Zhang, A. Joshi, M. Ma, V. Anisimov, and T. M. Rice, Phys. Rev. Lett. **85**, 1714 (2000).
[24] L. Paolasini, C. Vettier, F. de Bergevin, F. Yakhou, D. Mannix, A. Stunault, W. Neubeck, M. Altarelli, M. Fabrizio, P. A. Metcalf, and J. M. Honig, Phys. Rev. Lett. **82**, 4719 (1999).
[25] M. Sandri, M. Capone, and M. Fabrizio, Phys. Rev. B **87**, 205108 (2013).
[26] F. Iori, F. Rodolakis, M. Gatti, L. Reining, M. Upton, Y. Shvyd'ko, J.-P. Rueff, and M. Marsi, Phys. Rev. B **86**, 205132 (2012).
[27] D. Grieger, C. Piefke, O. E. Peil, and F. Lechermann, Phys. Rev. B **86**, 155121 (2012).
[28] I. Nebenzahl, Phys. Rev. **177**, 1001 (1969).
[29] M. Preisinger, J. Will, M. Klemm, S. Klimm, and S. Horn, Phys. Rev. B **69**, 075423 (2004).
[30] A. R. Oganov, J. Chen, C. Gatti, Y. Ma, Y. Ma, C. W. Glass, Z. Liu, T. Yu, O. O. Kurakevych, and V. L. Solozhenko, Nature (London) **457**, 863 (2009).
[31] Q. Zhang, X. Wu, and S. Qin, Chin. Phys. Lett. **29**, 106101 (2012).
[32] Y. Ding, C.-C. Chen, Q. Zeng, H.-S. Kim, M. J. Han, M. Balasubramanian, R. Gordon, F. Li, L. Bai, D. Popov, S. M. Heald, T. Gog, H.-k. Mao, and M. van Veenendaal, Phys. Rev. Lett. **112**, 056401 (2014).
[33] S. A. Corr, M. Grossman, J. D. Furman, B. C. Melot, A. K. Cheetham, K. R. Heier, and R. Seshadri, Chem. Mater. **20**, 6396 (2008).
[34] H. K. Mao, J. Xu, and P. M. Bell, J. Geophys. Res. **91**, 4673 (1986).
[35] M. Rivers, V. B. Prakapenka, A. Kubo, C. Pullins, C. M. Holl, and S. D. Jacobsen, High Press. Res. **28**, 273 (2008).
[36] G. Shen, P. Chow, Y. Xiao, S. Sinogeikin, Y. Meng, W. Yang, H.-P. Liermann, O. Shebanova, E. Rod, A. Bommannavar, and H.-K. Mao, High Press. Res. **28**, 145 (2008).
[37] J. Rodríguez-Carvajal, Physica B **192**, 55 (1993).
[38] A. C. Larson and R. B. Von Dreele, Los Alamos National Laboratory Report LAUR 86-748 (2004).
[39] S. Klotz, J.-C. Chervin, P. Munsch, and G. L. Marchand, J. Phys. D **42**, 075413 (2009).
[40] D. B. McWhan and J. P. Remeika, Phys. Rev. B **2**, 3734 (1970).
[41] Y. Sato and S.-i. Akimoto, J. Appl. Phys. **50**, 5285 (1979).
[42] L. W. Finger and R. M. Hazen, J. Appl. Phys. **51**, 5362 (1980).
[43] S. V. O. Dubrovinsky, D. M. Trots, A. V. Kurnosov, W. Morgenroth, H.-P. Liermann, and Leonid, J. Phys.: Condens. Matter **25**, 385401 (2013).
[44] See supplemental material at http://link.aps.org/supplemental/10.1103/PhysRevB.92.134106 for further analysis of experimental data and theoretical calculations.
[45] Y. Wang, J. Lv, L. Zhu, and Y. Ma, Phys. Rev. B **82**, 094116 (2010).
[46] Q. Li, Y. Ma, A. R. Oganov, H. Wang, H. Wang, Y. Xu, T. Cui, H.-K. Mao, and G. Zou, Phys. Rev. Lett. **102**, 175506 (2009).
[47] Q. Li, D. Zhou, W. Zheng, Y. Ma, and C. Chen, Phys. Rev. Lett. **110**, 136403 (2013).
[48] Y. Wang, J. Lv, L. Zhu, and Y. Ma, Comput. Phys. Commun. **183**, 2063 (2012).
[49] G. Kresse and J. Furthmüller, Phys. Rev. B **54**, 11169 (1996).
[50] Y. Guo, S. J. Clark, and J. Robertson, J. Phys.: Condens. Matter **24**, 325504 (2012).
[51] Y. Guo, S. J. Clark, and J. Robertson, J. Chem. Phys. **140**, 054702 (2014).